Mon. Not. R. Astron. Soc. **000**, 1–12 (2002) Printed 2 February 2008 (MN LATEX style file v2.2)

Disruption of a Dwarf Galaxy Under Strong Shocking: The Origin of ω Centauri

T. Tsuchiya[1,2⋆], V. I. Korchagin[3,5] and D. I. Dinescu[3,4]
[1] *Astronomisches Rechen-Institut, Mönchhofstraße 12-14, 69120 Heidelberg, Germany*
[2] *SGI Japan, Ltd., Yebisu Garden Place Tower, 4-2-3 Ebisu Shibuya-ku, Tokyo 150-6031, Japan*
[3] *Astronomy Department, Yale University,*
[4] *Astronomical Institute of The Romanian Academy*
[5] *Institute of Physics, Rostov-on-Don, Russia*

Accepted —-. Received —-.

ABSTRACT

We perform N-body simulations of the dynamical evolution of a dwarf galaxy falling into the Milky Way galaxy in order to understand the formation scenario of the peculiar globular cluster ω Centauri. We use self-consistent models of the bulge and the disc of the Milky Way, as well as of the dwarf galaxy, and explore a range of dwarf models with different density distributions. Namely, we use King (1966) and Hernquist (1990) density profiles to model the density distribution in the dwarf. The central region of our King model has a density profile approximately $\propto r^{-2}$, while that of the Hernquist model is $\propto r^{-1}$. The difference in the dwarf's density distributions leads to distinct evolutionary scenarios. The King model dwarf loses its mass exponentially as a function of apocentric distance, with the mass-loss rate depending on the initial mass and size of the dwarf. Regardless of the initial mass and size, the King model dwarf remains more massive than $10^8\ M_\odot$ after a few Gyr of evolution. The Hernquist model dwarf experiences an accelerated mass loss, and the mass of the remnant falls below $10^8\ M_\odot$ within a few Gyr. By exploring an appropriate set of parameters, we find a Hernquist model that can attain the mass and orbital characteristics of ω Cen after a few Gyr.

Key words: galaxies: dynamics and kinematics – galaxies: interactions – globular clusters: individual: ω Centauri – methods: N-body simulations

1 INTRODUCTION

The accretion and subsequent tidal disruption of dwarf galaxies are important agents in the formation and evolution of the Milky Way (Searle & Zinn 1978). Such accretion events would presumably lead to formation of tidal streams in the halo of the Milky Way associated with the disrupted dwarf galaxies. The discovery of the tidal stream related to the Sagittarius dwarf galaxy (Ibata et al. 2001) indeed supports the idea that halos of galaxies can have a number of streams maintaining their coherence during a few Gyrs.

There is another class of halo objects which might be associated with past accretion events. During the accretion of nucleated dwarf elliptical galaxies, the compact stellar nuclei may survive the disruptive event and continue orbiting until the present time. Freeman & Bland-Hawthorn (2002) even speculate that the globular clusters in the Milky Way could be the stripped relics of ancient protogalactic stellar systems. To identify such objects would be of great importance in understanding the nature of such building blocks of galaxies. In this paper we focus on one object which may be the relic of a past accretion event - the globular cluster ω Centauri. ω Centauri is one of the most peculiar globular clusters in the Milky Way: with a mass of $5 \times 10^6 M_\odot$, it is the most massive globular cluster. It has an unusual flatness with an ellipticity of about 0.12 associated with fast internal rotation (Freeman 2001). It orbits in a retrograde direction relative to the disc with an apocentric radius of about 6 kpc, a pericentric radius of 1.2 kpc, and a maximum height above the plane of 1 kpc (Dinescu et al. 1999).

What really distinguishes ω Cen from other Galactic globular clusters, is its chemical abundance pattern. It is the only known globular cluster that has well-defined signatures of self-enrichment. Thus, according to Smith et al. 2000 and Vanture et al. 2002, the abundance pattern observed within ω Cen can be understood as a combination of Type II super-

⋆ e-mail: tsuchiya@ari.uni-heidelberg.de

novae and, more importantly, AGB-star enrichment during a period of about 3 Gyr. Gnedin et al. (2002) have demonstrated that ω Cen on its present orbit and with its present mass can not retain heavy elements dispersed in the AGB phase of stellar evolution. The passages through the disk would sweep out the intracluster gas and the cluster, once established on this orbit, would not be able to produce stars with enhanced s-process elements. Thus, the cluster should have evolved chemically before settling on its present orbit, or, in other words, it was accreted by the Galaxy. Another possibility to explain the chemical peculiarities of ω Cen is the merger of two or more chemically distinct systems. Vanture et al. (2002) conclude however, that in this scenario, it would be difficult to explain an increase in the of ratio of heavy s-process elements to iron with metallicity.

A plausible explanation is that ω Cen is the nucleus of a dwarf galaxy captured and disrupted by the the Milky Way (e.g., Freeman 1993). In this scenario, a dwarf sinks to the center of the Galaxy due to dynamical friction, simultaneously losing mass in the Galactic tidal field. All of the dwarf's mass is eventually stripped but the nucleus, with a mass of 5×10^6 $M_\odot$, is left on the current orbit of ω Cen. The current angular momentum of ω Cen is thus inherited from the dwarf galaxy, on a retrograde orbit. The complex chemical composition and extended star formation history of ω Cen can be explained in this picture by the chemical evolution of the nucleus in a deep potential well of a dwarf, such that the nucleus would be able to retain stellar ejecta during subsequent activity of supernovae and AGB stars.

Even though a capture scenario is seen as a plausible explanation for the peculiar properties of ω Cen, it is unclear whether it is possible to realize an orbit and mass evolution of the dwarf that can reproduce the current parameters of ω Cen. Zhao (2002) studied the orbital decay of a dwarf that may lead to the current position of ω Cen by launching a dwarf on an orbit that started 50 kpc away from the Galactic center. Using a semi-analytical model, he concluded that a progenitor of ω Cen can not decay to its present orbit. He found that strong tidal shocks quickly reduce the mass of the dwarf so that dynamical friction becomes too weak to drag the remnant to the inner regions of the Galaxy. Zhao (2002) concluded that the only possibility to explain ω Cen - phenomenon is that its progenitor was born only 15 kpc away from the Galactic center.

Zhao's analysis, however, was simplified in a number of ways. He assumed that the mass outside the tidal radius is instantaneously stripped, and the contribution from the bulge and disc components to the dynamical drag was not taken into account. In this study, we perform a series of numerical simulations, using self-consistent bulge and disc models for the Milky Way, and self-consistent dwarf models that have different density profiles. As a result, we find a dwarf-capture scenario that successfully produces an ω Cen-like object from a normal dwarf galaxy. This result is also reported in more detail in a separate paper (Tsuchiya et al. 2003). In this paper, we explore the model parameters and focus on the physical processes of the dynamical evolution of such infalling dwarfs making this study beneficial in understanding the properties of merging parent-satellite galaxy systems.

The numerical realization of this scenario is a complicated problem because of the large range of masses and sizes of the interacting components, and due to the drastic change of the mass of the sinking dwarf. We explain our numerical methods in Sect. 2, where we describe the Galaxy and the dwarf models. The results of the simulations are presented in Sec. 3. Some analytical considerations for our results are given in Sect. 4. Finally we formulate our conclusions in Sect. 6.

2 MODELS AND NUMERICAL METHODS

2.1 N-body simulations

In our N-body simulations, we neglect gaseous effects such as pressure and viscosity. We do not include star formation, and do not distinguish between visible and dark matter in the models. Gravitating matter is represented by the softened particles, and their mutual gravity is calculated by a hierarchical tree algorithm (see, for example Dubinski (1996) for a review). The tolerance parameter which is used to organize the hierarchical boxes, is 0.7. The softening length is 0.01 of the disc scale length, which corresponds to 35 pc in our Milky Way model. We use the same value of the softening length for all particles irrespective of their mass.

The integration time step is 1/32 of the dynamical time which is determined as the quarter of the orbital period of a particle at the center of the Milky Way. This gives a value of 4.38×10^5 years. The central density of our dwarf is an order of magnitude larger than that of the Milky Way model. However, the orbiting time of the stars in the dwarf is longer compared to the time step.

An oscillation time of the dwarf in the potential of the Milky Way is about 0.5 Gyr at the beginning of an infalling process, and about 0.1 Gyr at later stages of evolution. Since the plane of the orbit of the dwarf has a low inclination with respect to the disc, a characteristic time of the gravitational shocking from the disc is comparable to the dwarf's orbiting time. The bulge shocking time determined as a time of crossing of the bulge by a moving satellite is much shorter (about 3×10^6 years) compared to the gravitational shoking time from the disk, making bulge shocking much stronger.

2.2 The Milky Way Model

An accurate model of the Milky Way is important to make a quantitative estimate of the dwarf evolution. We construct the Milky Way equilibrium model following Kuijken and Dubinski (1995). The model provides wide flexibility in fitting observational constraints. Briefly, it consists of a nearly spherical bulge, an exponential disc, and a halo which resembles a lowered isothermal sphere at larger scales. Each component is expressed by a distribution function, so that the positions and the velocities of N-body particles can be directly sampled from the distribution functions. Since the model is close to equilibrium, there is no need to "relax" it before an actual simulation.

The parameters of the model are chosen to reproduce the properties of the real Milky Way galaxy. We choose the solar radius, the disc exponential scale length (R_d), and the disc vertical scale height (z_d) to be 8 kpc, 3.5 kpc, and 245pc respectively. The circular velocity of the disc at the solar radius is taken to be 220 km/s. The total surface density

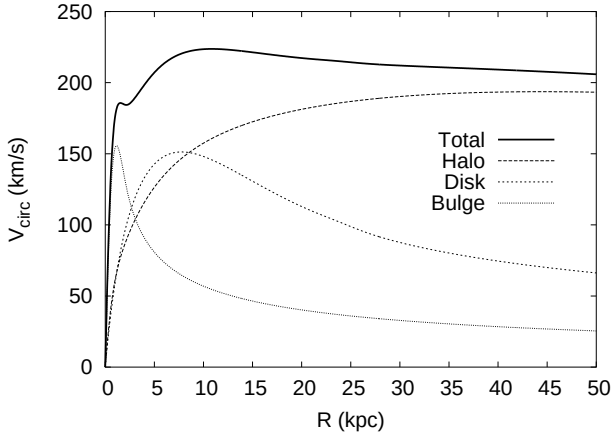

Figure 1. The rotation curve of our Milky Way model. The contributions from the bulge, disc and halo to the circular velocity are shown by dotted, short-dashed, and long-dashed curves, respectively.

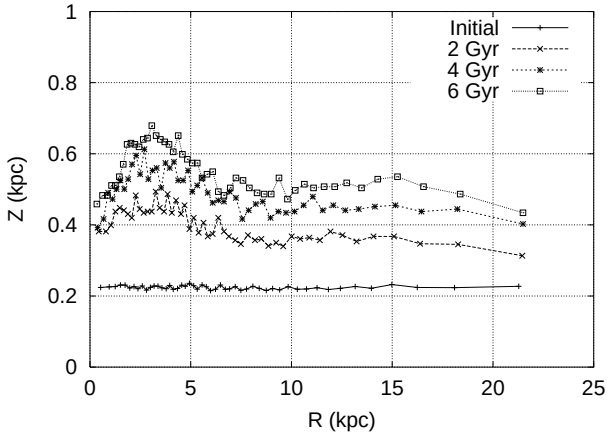

Figure 2. Artificial heating of the Milky Way disc model due to two-body relaxation. The number of particles in the bulge and disc components is 10,000 and 70,000 respectively, and the halo is treated as a fixed potential. The softening length in the tree code is 35 pc.

within 1.1 kpc of the disc plane, and the contribution of the disc material to it are 69.8 $M_\odot$ pc^{-2}, and 45.5 $M_\odot$ pc^{-2} respectively, which agrees with the observational constraints of 71 ± 6 $M_\odot$ pc^{-2} and 48 ± 9 $M_\odot$ pc^{-2} (Kuijken and Gilmore 1991). With a cut-off radius of 28 kpc, the disc total mass is 5×10^{10} $M_\odot$. Toomre's Q value of the disc is about 1.9 at a distance of 2.5 R_d from the center. The bulge mass and the cut-off radius of the bulge are taken to be 0.75×10^{10} $M_\odot$ and 2.38 kpc respectively.

The halo density distribution can be well approximated by a spherical lowered isothermal profile (Binney and Tremaine 1987) with a central potential $\Psi(0)/\sigma^2 = 8$ except for the central regions which are deformed owing to the presence of the bulge and the disc. The halo mass inside 50 kpc and 170 kpc radii is 4.9×10^{11} $M_\odot$ and 8.6×10^{11} $M_\odot$ respectively. This is within the observationally inferred values $5.4^{+0.2}_{-3.6}\times10^{11}$ $M_\odot$ and $1.9^{+3.6}_{-1.7}\times10^{12}$ $M_\odot$ found by Wilkinson and Evans (1999). The contribution of each component to the circular velocity is shown in Fig. 1.

This model is similar to model S in Tsuchiya (2002). An interested reader can find in that paper a more detailed description of the model and its stability analysis. The bulge and the disc in our sumulations are represented by 10,000 and 70,000 equal mass particles. With this rather low number, the disc thickness grows due to two-body relaxation. Fig. 2 shows the change in the disc thickness in equilibrium. During 6 Gyrs, the disc thickness increases up to 500 pc near $R = 10$ kpc. This is about twice as large as the present day thin disc, but smaller than the scale height of the thick disc. The bump in the disc thickness around $R = 3$ kpc is caused by a weak bar developing in the disc. A further discussion of this effect can be found in Tsuchiya (2002).

In this study, the halo is treated as a fixed potential since we are mainly interested in the effects of the disc and bulge shocking and dragging of the dwarf galaxy. We neglect dynamical friction from the halo in our models, which increases the orbital sinking time (see also Section 5.1). If we treat the halo as an ensemble of N particles, additional heating causes disc thickening. To prevent considerable disc heating, the number of particles in the halo should be several times larger than that in the disc. This implies severe limitations on our computational capabilities. Nevertheless we run one simulation with a "living" halo to estimate the contribution of the halo to the dwarf's dynamics. The halo dynamical friction decreases the dwarf's orbital decay time and increases its mass loss, but does not change the evolution history in the mass–apocenter radius plot. We discuss this issue in section 5.1.

2.3 Dwarf Models

We assume that a dwarf galaxy captured by the Milky Way was the hypothetical progenitor of ω Cen. Presumably, a high-density nucleus of the dwarf survived the disruptive capture event and ended as ω Cen. We wish thus to explore dwarf models with centrally concentrated density profiles. We examine two models: the lowered isothermal or the King model (Binney and Tremaine 1987), and the Hernquist model (Hernquist 1990). Both models are spherically symmetric. The kinematics of the compact dwarf spheroidal galaxies does not reveal a significant rotation of these systems (Binney & Merrifield 1998). We assume therefore that both of our models have no rotation. The King model is defined by the distribution function

$$f_{\rm K}(\varepsilon) = \begin{cases} \rho_1(2\pi\sigma^2)^{-3/2}\left(e^{\varepsilon/\sigma^2}-1\right) & \varepsilon > 0; \\ 0 & \varepsilon \le 0, \end{cases} \qquad (1)$$

where $\varepsilon = -\frac{1}{2}v^2 + \Psi$ is a specific relative energy of the particles defined so that the energy is zero at the surface with zero volume density. The value of the dwarf potential at the center, $\Psi(0)$, determines how centrally concentrated the distribution is. We adopt the value $\Psi(0)/\sigma(0)^2 = 12$.

The model has two characteristic scale lengths: the King radius $r_K \equiv \sqrt{9\sigma_0^2/4\pi G\rho_0}$, and the tidal radius r_t. For $\Psi(0)/\sigma_0^2 = 12$, the ratio between the tidal and the King radii, is $r_t/r_K = 548$. These two scale lengths are

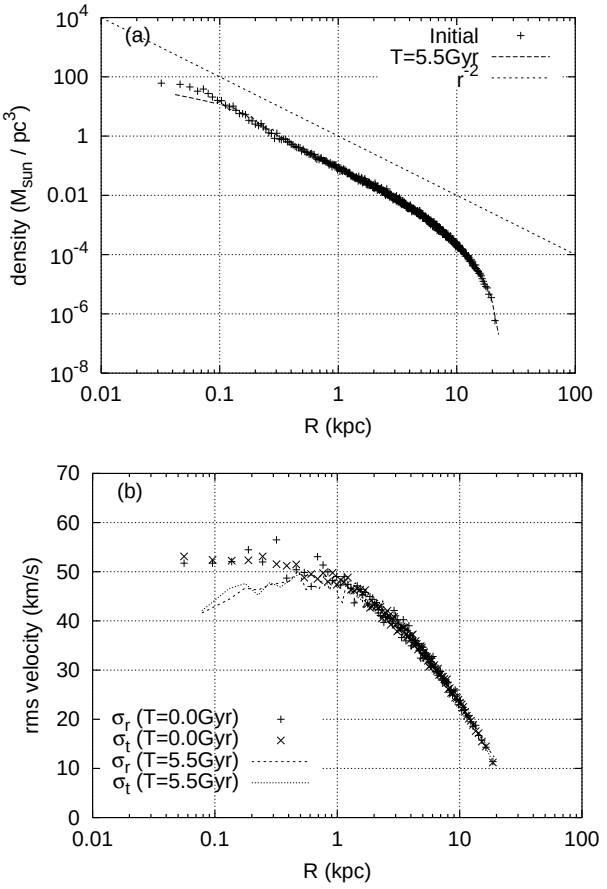

Figure 3. Density distribution (upper panel) and velocity dispersion (lower panel) in the King model with $\Psi(0)/\sigma_0^2 = 12$. The total mass and the half-mass radius of the model are 8×10^9 $M_\odot$ and 4 kpc respectively (model K5). The distribution is taken from our N-body realization with $N = 50,000$ particles averaged over spherical shells containing 100 particles for the density distribution, and 1000 particles for the rms velocity distribution. The dashed line in the upper panel shows the density distribution in the model after 5.5 Gyr of evolution in isolation. For comparison, we also show the r^{-2} density distribution (dotted line). In the lower panel, the dashed and dotted lines show the radial and the tangential velocity dispersion profiles respectively, after 5.5 Gyr evolution of the model in isolation.

not convenient however, for the comparison with the Hernquist models, so we label the distributions by their half-mass radii related to the King radius and the tidal radius as $r_{1/2} = 0.164 r_t = 89.9 r_K$. Figure 3 shows the density and velocity profiles in our King model with total mass 8×10^9 $M_\odot$ and half-mass radius $r_{1/2} = 4$ kpc sampled by 50,000 particles. Since the model has a deep central potential, a few hundred particles compose the central homogeneous core of the dwarf.

To study the numerical stability of the model, we have followed its evolution in isolation for about 5.5 Gyr. The final distributions are shown in Fig. 3. The central density decreases by a factor of 2. The change in density profile is noticeable within $r < 0.1$ kpc of the dwarf center which contains mass of about 10^8 $M_\odot$. The central velocity dispersion decreases by about 25%, while there is no considerable change in the velocity dispersion profile in the outer regions of the dwarf, i. e., at $r > 0.5$ kpc.

The Hernquist model (Hernquist 1990) has a density profile given by the equation

$$\rho(r) = \frac{M_{\rm tot} r_0}{2\pi r (r + r_0)^3}. \quad (2)$$

In central regions, the density profile has a cusp of r^{-1}, while in the outer regions the density decreases as r^{-4}. The radius r_0 separating the two regions is related to the half mass radius as:

$$r_{1/2} = (1 + \sqrt{2}) r_0. \quad (3)$$

The slope of the density gradient in the central region is thus shallower than that in the King models.

A more noticeable difference between the two models is in their velocity dispersion profiles. While the King models have constant velocity dispersion in the center, in the Hernquist models the velocity dispersion decreases near the center as $\sigma^2 \propto r/r_0 \ln(r_0/r)$ (Hernquist 1990). Figure 4 shows a realization of the Hernquist model which has a total mass of $M_{\rm tot} = 8 \times 10^9$ $M_\odot$ and half-mass radius of $r_{1/2} = 2\sqrt{2}$ kpc. This Figure also shows the density and the velocity dispersion profiles after 5.5 Gyr evolution in isolation. The density in the central region, within the softening length, decreases in the same way as for the King model. However, the velocity dispersion profiles remain close to the initial disrtributions.

Evolution of the dwarf's central regions is caused by the softening of the gravity forces. As can be seen from Figure 3, the velocity dispersion profile in the King models flattens toward the center, while the volume density grows faster than r^{-2}. To keep the central regions in equilibrium, the self-gravity force in the King models should grow towards the center. The velocity dispersion in equilibruim Hernquist models decreases toward the center(Figure 4), which results in a constant self-gravity force in the central regions. The softening length of 35 pc is comparable to the King radius of 44.5 pc. Thus, the gravity softening decreases the gravity force in the core regions, and causes the core to expand reducing its density and velocity dispersion. Central regions of our numerical King equilibrium models with softened gravity are more departed from equilibrium than those of Hernquist models, which results in more noticeable evolution of central regions of the King models.

Decreasing the density at the center of the dwarf can potentially cause its more rapid disruption. We find however, that the mass of the King models remains larger than 10^8 $M_\odot$ during the simulations and a structural change at the dwarf center does not affect mass stripping in the simulations. Our test simulations thus show that isolated dwarf models are fairly stable at scales larger than a few softening lengths. In other words, artificial effects such as the softening and the two-body relaxation do not affect the mass stripping history unless the mass of the remnant falls below 10^7 $M_\odot$.

2.4 Multi-Mass N-Body Model of the Dwarf

With our choice of the softening length, the numerical resolution near the dwarf's center is about 10^7 $M_\odot$. In our King models, we use 50,000 particles to represent a 8×10^9 $M_\odot$ dwarf, and a 10^7 $M_\odot$ object would consist of a few tens of

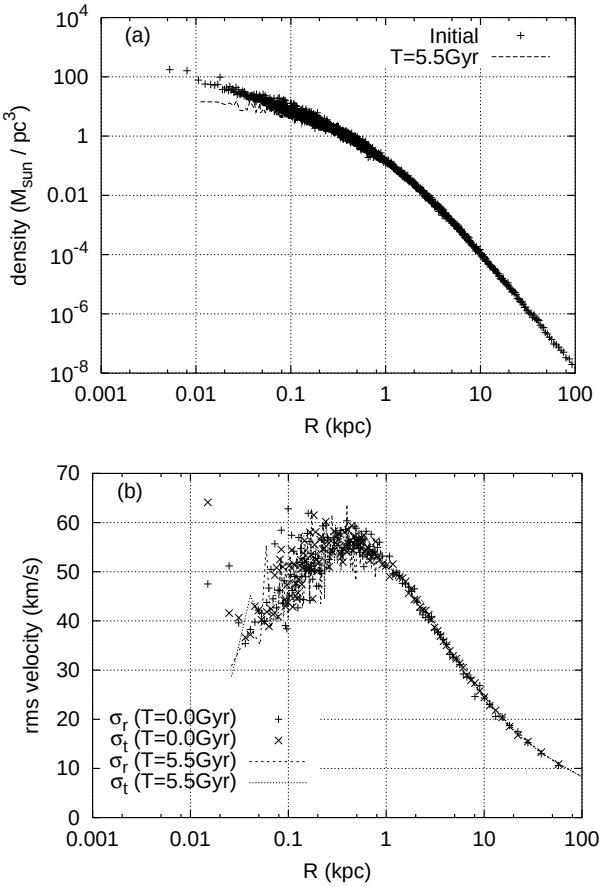

Figure 4. Density (upper panel) and velocity dispersion (lower panel) distributions for the Hernquist model with total mass of 8×10^9 $M_\odot$ and the half mass radius of 2.83 kpc (model H5) taken from multi-mass N-body realization with $N = 140,000$ particles. The density distribution is determined from averages over spherical shells that contain 100 particles each, while the velocity dispersion distribution from shells that contain 1000 particles. The dashed line in the density plot represents the distribution of the model after 5.5 Gyr of evolution in isolation. The lines in the velocity dispersion plot show the radial (dased) and tangential (dotted) velocity dispersions after 5.5 Gyr of evolution in isolation.

particles. To improve mass resolution, we increase the number of particles close to the dwarf center. We find that the Hernquist models undergo strong mass loss, and the mass of the remnant becomes less than 10^7 $M_\odot$ during a few Gyr while the King model dwarfs stop losing their mass above 10^8 $M_\odot$. To avoid effects caused by a small number of particles at the late stages of evolution, a remnant should be composed of more than a thousand particles. To increase the mass resolution of the Herquist model near the center, we use a mulyi-mass N-body model of the dwarf. We divide the particles in the model into three groups differing by their energy:

$$\begin{aligned} \int_{E\le E_1} f_{\rm H}(E) d\boldsymbol{x} d\boldsymbol{v} &= 0.01, \\ \int_{E_1<E\le E_2} f_{\rm H}(E) d\boldsymbol{x} d\boldsymbol{v} &= 0.09, \\ \int_{E_2<E} f_{\rm H}(E) d\boldsymbol{x} d\boldsymbol{v} &= 0.9, \end{aligned} \tag{4}$$

where $E = \frac{1}{2}v^2 + \Phi(\boldsymbol{x})$ is a specific energy of the individual particles. The lowest energy group is sampled by the particles with mass $m_1 = 2 \times 10^{-7} M_{\rm tot}$, and with the number of the particles in the group equal to 50,000. The middle and the high energy groups are sampled by the particles with masses $m_2 = 2 \times 10^{-6} M_{\rm tot}$ and $m_3 = 2 \times 10^{-5} M_{\rm tot}$ respectively, and with the number of particles in each group of 45,000. Since the light particles are progressively concentrated near the center, the mass resolution of the dwarf central regions becomes about a hundred times better. The central 10^7 $M_\odot$ for example is composed now of more than 50,000 particles.

A potential problem of N-body models with different masses of particles is an artificial heating of light particles. In our model, light particles are concentrated toward the dwarf's center, while heavy particles are distributed at the periphery of the dwarf. On the contrary, in a dwarf close to equilibrium, massive particles sink toward its center, while light particles are scattered away. In other words, there is a net energy flow from the massive particles to the light ones in our model. We have checked whether this process is significant in our simulations. Fig. 5 shows energy exchange between particles of different masses as a function of time for the equilibrium multi-mass Hernquist model evolving in isolation. Solid, dashed and dotted lines in this Figure stand for the low, medium and high mass particles. The left panel in Fig. 5 shows the total energy of each group of particles as a function of time, while the right panel shows the specific energy, averaged over the particles in each component. Ninety percent of the mass of the dwarf in our model is built with massive particles. Therefore the specific energy of heavy particles does not change significantly, while the total energy does.

There is no noticeable relaxation between the low and intermediate mass particles. The global energy flow is dominated by the energy transfer from heavy to the intermediate and low-mass particles with the dominant energy exchange being between the massive and intermediate mass ones. The light particles also gain energy as a result of relaxation. This energy gain, although, does not cause a significant change in the equilibrium density ditribution as can be seen in Figure 4. Furthermore, heating of the light particles is even less important in our simulations since most of the heavy particles are stripped away from the dwarf at early stages of the infalling process.

2.5 Bound mass

The bound mass of a dwarf moving in an inhomogeneous background field is a rather ambiguous quantity. One way to determine the dwarf's bound mass is to calculate the total mass of the dwarf particles that have negative energy, ignoring the external gravitational field of the Milky Way:

$$E_{\rm SG}^{(i)} = \frac{1}{2} m_i v_i^2 + \Phi_{\rm dwarf}(\boldsymbol{x}_i) \le 0. \tag{5}$$

Another way is to calculate the mass inside the tidal radius where the tidal force from the Milky Way is comparable to the self-gravity of the dwarf. This would be an

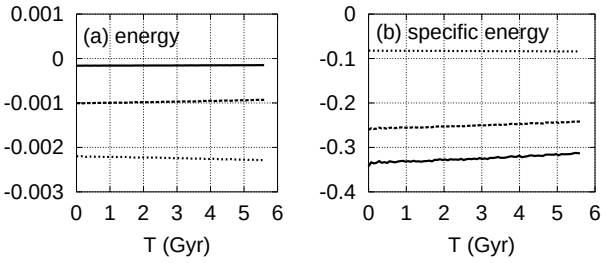

Figure 5. Energy change in the three different mass components of the multi-mass Hernquist dwarf. Panel **(a)** shows the total energy of each component, while panel **(b)** shows the specific energy averaged over the particles in each component. The solid, dashed, and doted lines stand for the light, medium, and heavy mass components respectively.

appropriate bound mass definition if the dwarf is subject to a strong tidal field. To simplify the tidal radius calculations, we assume that the Milky Way is spherically symmetric with a homogeneous core of 1-kpc radius, and has a flat rotation curve of 220 km/s outside the core region. We use the expression for the tidal radius from Binney and Tremaine (1987) ignoring the deviation of the Milky Way from spherical symmetry:

$$r_t = \left(\frac{M_{\rm dwarf}(r_t)}{3M_{\rm MW}(d)} \right)^{1/3} d, \tag{6}$$

Here, d is the distance between the center of the dwarf (defined at the location of the minimum of the dwarf's potential) and the center of the Milky Way, $M_{\rm dwarf}(r_t)$, and $M_{\rm MW}(d)$ are the mass of the dwarf within the tidal radius, and the mass of the Milky Way within radius d. Under these assumptions, the dwarf tidal mass is determined by the expression:

$$\frac{M_{\rm dwarf}(r_t)}{r_t^3} = \begin{cases} 3.27\times10^{10}\left(\frac{V_{rot}}{220{\rm kms}^{-1}}\right)^2\left(\frac{M_\odot}{\rm kpc^3}\right) & d \le 1 \text{ kpc} \\ \frac{3.27\times10^{10}}{(d/1\text{ kpc})^2}\left(\frac{V_{rot}}{220{\rm kms}^{-1}}\right)^2\left(\frac{M_\odot}{\rm kpc^3}\right) & d > 1 \text{ kpc} \end{cases} \tag{7}$$

As a practical compromise, we also calculate gravitationally bound mass of the dwarf within its tidal radius. Fig. 7 shows the bound mass of an infalling dwarf as a function of time defined in this way, as well as the bound mass calculated with the other two definitions. The bound mass determined within tidal radius of the dwarf does not have peculiar features observed in the mass profile calculated for the mass of the remnant bound by its self-gravity.

3 RESULTS

This section presents the results of the numerical simulations of the infall of a dwarf that has King and Hernquist density profiles. To match approximately the current orbit of ω Cen, the initial position and velocity of the dwarfs have been choosen to be $(X, Y, Z) = (50, 0, 30)$ kpc, and $(V_X, V_Y, V_Z) = (0, -20, 0)$ km/s. Here X, Y, Z are the Cartesian coordinates associated with the Galaxy, X is positive away from the Galactic center, Y is positive in the direction of the Galactic rotation, and Z is positive toward the North Galactic pole. The total masses and the half mass radii of the examined models are listed in Table 1 for the King models, and in Table 2 for the Hernquist models. These parameters control the overall evolution of the dwarf. Massive dwarfs sink faster in the potential well of the Milky Way, while dwarfs with the large half-mass radii, i.e. a lower volume density experience more rapid mass loss.

Table 1. Parameters of the King models

Model No.	$M_{\rm tot}$ ($M_\odot$)	$r_{1/2}$ (kpc)	N
K1	4×10^9	1.0	50000
K2	4×10^9	2.0	50000
K3	4×10^9	4.0	50000
K4	8×10^9	2.0	50000
K5	8×10^9	4.0	50000
K6	8×10^9	8.0	50000

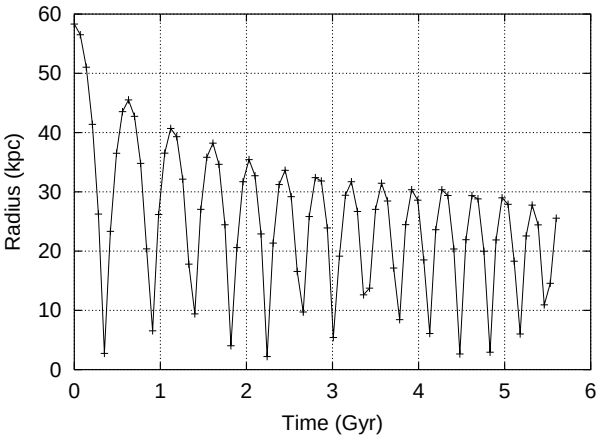

Figure 6. Time evolution of the orbital radius of the dwarf model K5.

The King models (K1, K4), (K2, K5) and (K3, K6) listed in Table 1 are related to each other as

$$M_{\rm dwarf}/r_{1/2} = \text{const.} \tag{8}$$

With the density profile of King models close to $\rho \propto r^{-2}$, the pairs of models have the same radial density distributions, and implicitly same central densities. Thus, pair (K1, K4) has the highest central density, while (K3, K6) has the lowest central density. The Hernquist models (H1, H4, H7), (H2, H5, H8) and (H3, H6, H9) listed in Table 2, are related as

$$M_{\rm dwarf}/r_{1/2}^2 = \text{const.} \tag{9}$$

Similarly to the King models, these models have the same density distribution and therefore central density within each group. Group (H1, H4, H7) has the highest central density, while group (H3, H6, H9) has the lowest.

3.1 King Models

All the King models listed in Table 1 are composed of 50,000 identical particles and have central potential depth of $\Psi(0)/\sigma_0^2 = 12$.

Figure 6 shows the time evolution of the dwarf orbit for model K5 taken as an example. This plot shows the distance of the dwarf from the center of the Milky Way as a function

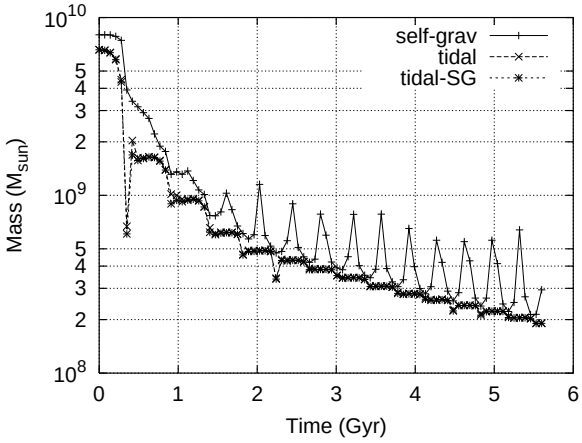

Figure 7. The mass of the dwarf model K5 as a function of time. The solid and dashed lines show the mass of the dwarf calculated as gravitationally bound and tidal mass respectively. The dotted line is the bound mass determined as gravitationally bound mass of the dwarf within its tidal radius.

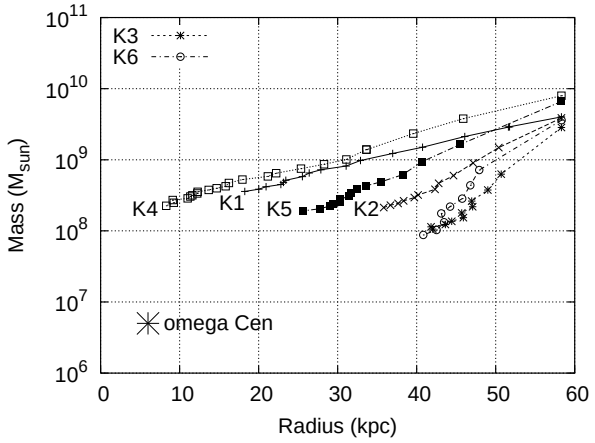

Figure 8. Evolution of the mass as a function of apocentric distance for the King models. The labels in Figure match the models listed in Table 1.

of time with the position of the dwarf determined as the point where the dwarf potential reaches its minimum.

The dwarf has a highly eccentric orbit which decays due to the interaction with the disk and the bulge of the Milky Way. The distance minima in Figure 6 do not correspond to the exact pericentric passages of the dwarf because of the rather low time resolution in the plot, that is about 700 Myr. We estimate the typical dwarf's pericentric distances of about 1 kpc.

Fig. 7 shows the mass loss history for the dwarf model K5. We use three different definitions of the dwarf's bound mass. The dashed line shows the mass of the dwarf within its tidal radius. The dotted line shows the behavior of the gravitationally bound mass of the dwarf within its tidal radius. For comparison, we plot also the mass of the gravitationally bound particles of the whole dwarf (solid line). The mass of the remnant determined by the gravitationally bound particles is larger than the mass of the remnant within its tidal radius. Until t $\sim$ 1.4 Gyr, the mass of gravitationally bound particles of the dwarf decreases monotonically, changing later on into an oscillatory regime. By defining the remnant mass as the mass of the dwarf's gravitationally bound particles, we neglect the gravity of the Galaxy. With this definition, the particles with sufficiently small velocities will be gravitationaly bound even if they are located at large distances from the dwarf center. Close to apocenter, the dwarf and the stripped particles slow down, which results in an increase of the dwarf bound mass. We find this definition inappropriate for our problem.

The mass of the remnant determined by its tidal radius changes mainly during its pericentric passages and remains nearly constant for the rest of the orbiting time. A simple approximation for the tidal radius estimate is invalid however close to pericenter, where the dwarf's distance from the Galactic center is comparable to the size of the dwarf itself. The bound mass determined as a mass of gravitationally bound particles within the tidal radius ofthe dwarf is thus the most plausible definition of the gravitationally bound mass for our problem.

The orbital sinking of the dwarf is caused by dynamical friction, or a back reaction from the disc and bulge density perturbations determined by the dwarf's gravitaty. In an ideal case, the drag force is proportional to the square of the dwarf mass (Chandrasekhar 1943). As the dwarf loses its mass, the orbital decay rate decreases. The history of the orbital decay depends thus crucially on the mass loss rate of the dwarf, which in turn depends on dwarf's internal density distribution. We study these complex connections in an evolutionary history of the dwarf by a systematic parameter survey of our models.

An illuminating diagram is Figure 8 which shows the bound mass as a function of apocentric distance of the dwarf. The evolution history of King dwarf models can be classified into the three groups depending on their initial central density. Models in each pair, e.g, (K1, K4), (K2, K5), and (K3, K6) reach nearly the same bound mass and apocentric distance in their evolutionary courses. These model pairs have the same density distributions, and once the outer parts of the dwarf are stripped, the models in each pairs have nearly identical remnants. The bound mass of the King model dwarfs decreases exponentially with apocentric radius. An extrapolation of the evolution of model K2 could lead in principle to a remnant with the mass and the orbital parameters close to those of ω Cen. However, the evolution time to reach ω Cen's parameters is larger than the age of the Galaxy, and ω Cen's origin can not be explained by this model.

Figure 8 also illustrates a common evolution of the models that have the same central densities. Models K2 and K5, for example, have close masses by the second pericentric passages. Models K3 and K6 have close bound masses even at the beginning of the simulations since this pair of models has the lowest central density, and the tidal radius for these models is already small at $R \sim 60$ kpc. The additional initial mass in model K6 compared to the model K3 is distributed outside the tidal radius (as defined in Section 2.5), and is stripped during the very first passage by the Galactic center.

Figure 9 illustrates the mass evolution of the King dwarf models. By 6 Gyr, the most the dwarf models reach mass of about few$\times 10^8$ $M_\odot$, with the mass loss comparable with that found in Zhao' model (Zhao 2002). Although the models K3

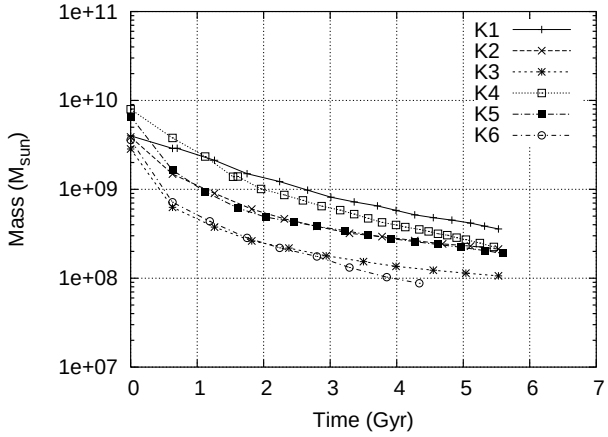

Figure 9. Evolution of the mass of the King dwarfs as a function of time.

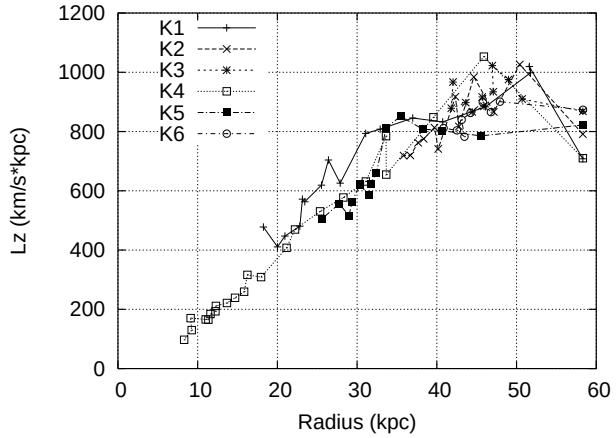

Figure 10. Evolution of the angular momentum as a function of the decaying apocentric radius of the King dwarfs.

and K6 have higher mass loss rates and reach 10^8 $M_\odot$ during 4 Gyr of evolution.

A similar evolutionary pattern among different King models can be seen also in dependence of the specific angular momentum L_z. Fig. 10 shows Lz with the apocentric radius. The positive L_z is for retrograde orbits to the disc rotation. At the beginning, we set the same orbital parameters for all models so that all models have the same initial L_z.

3.2 Hernquist Models

To examine the dynamics of the Hernquist model dwarfs, we build nine models listed in Table 2. As it was mentioned before, there are three groups of models namely (H1, H4, H7), (H2, H5, H8), and (H3, H6, H9) which differ in their half-mass radii and mass but have the same radial density distributions (i. e., central densities).

Figure 11 shows mass evolutionary tracks for the nine Hernquist models. In this Figure, the bound mass of the remnant is plotted as a function of its apocentric distance. Similarly to the King models, a common behavior of the Herquist models which have the central density is seen in

Table 2. Parameters of the Hernquist models

Model No.	$M_{\rm tot}$ ($M_\odot$)	$r_{1/2}$ (kpc)	N
H1	4×10^9	1.0	140000
H2	4×10^9	2.0	140000
H3	4×10^9	4.0	140000
H4	8×10^9	1.414	140000
H5	8×10^9	2.828	140000
H6	8×10^9	5.657	140000
H7	16×10^9	2.0	140000
H8	16×10^9	4.0	140000
H9	16×10^9	8.0	140000

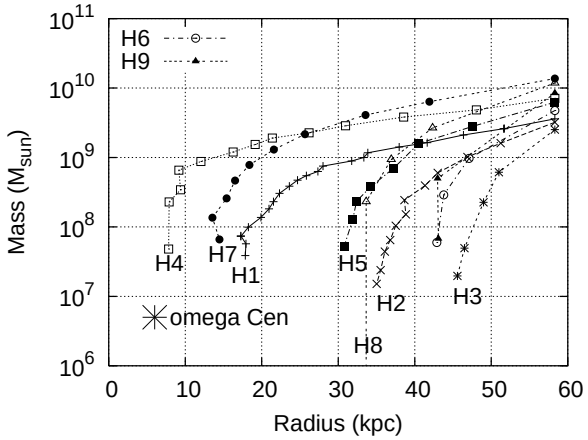

Figure 11. Evolution of the mass of Hernquist dwarf models as a function of dwarf's apocentric radius.

Figure 11. Once the tidal interaction strips the outer layers of a dwarf belonging to the same group, the remnants become nearly identical and have close orbital behavior.

A difference in the behavior of the Hernquist models when compared to the King models is the bending of the evolutionary tracks at lower masses. The decay of the apcentric radius stops in both models, but the Hernquist model dwarfs continue to loose their mass after the orbit evolution is terminated. All of the models but H1 are completely disrupted in our simulations during a finite time.

The central mass distribution of a dwarf can not always be represented by the Hernquist profile. The center of a dwarf may have a much denser nucleus or even a black hole. In this case, the dense central parts of the dwarf may survive the disruptive gravitational shocks and settle on a low-energy orbit of apocentric radius smaller than the Solar circle for instance, or even settle within the bulge of the Galaxy. Our simulations follow the mass evolution of the dwarf until the mass of the remnant is about few $\times 10^7$ $M_\odot$. As it is seen from Fig. 11, the dwarf orbits stop their decay when the mass of the remnant is below 10^8 $M_\odot$. Therefore, regardless the mass evolution of the dwarf at the very final stages, a hypothetical central object will be launched at the dwarf orbit when mass of the remnant is about 5×10^7 $M_\odot$. The parameters of the final orbit of the central nucleus of the dwarf can be estimated rather firmly. In particular, the central nucleus of the Hernquist dwarf which has the high volume density will have an orbit with apocentric distance

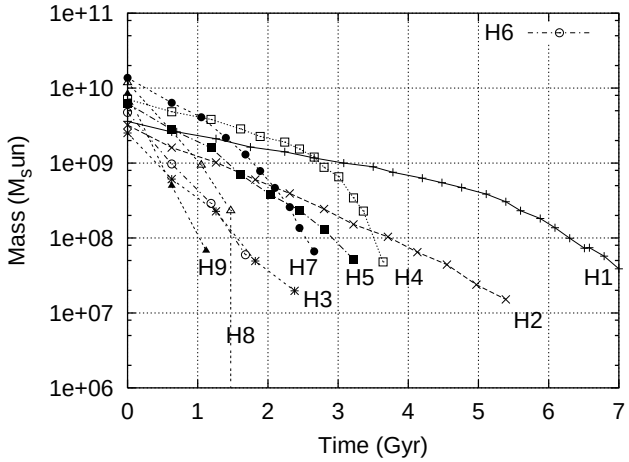

Figure 12. Evolution of the bound mass of the Hernquist dwarfs as a function of time.

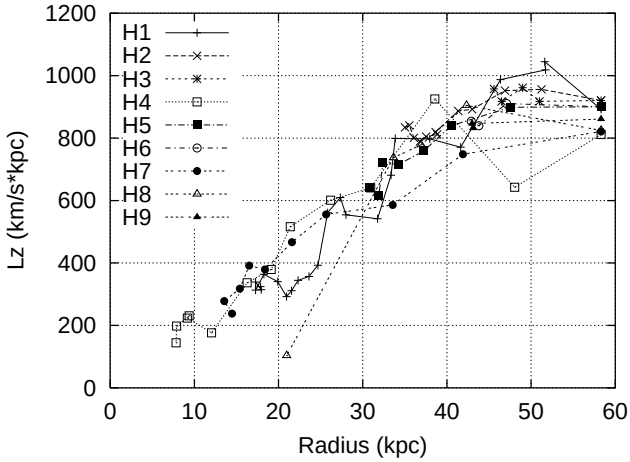

Figure 13. Evolution of the angular momentum as a function of the decaying apocentric radius of the Hernquist dwarfs.

of $10 \sim 20$ kpc. Remarkably, model H4 sinks to the Galactic center with apocentric radius of 6 kpc which is close to an apocentric distance of ω Cen. It has to be noticed, however, that a progenitor galaxy has to contain in its center a comparact self-gravitating nucleus which can survive disruptive encounters with the bulge and the disk of the Milky Way.

The disk thickening due to an artificial heating, and due to an interaction with the satellite can affect the orbit decay. This effect depends though on the satellite orbit. In our simulations which model the origin of Omega Centauri, the orbit decay occurs during first 2 Gyr, or during five-six dwarf revolutions around the Milky Way center (Tsuchiya et al. 2003). We find that during this time, the satellite orbit is not co-planar with the Milky Way disk, and the dwarf spends a short time inside the finite thickness disk of the Milky Way. In other words, the disk remains 'thin' for the dwarf, and the gravitational drag force acting at every point of the dwarf orbit does not change much compared to the drag force for the disk with the fixed thickness.

The final apocentric distance of the nucleus is not a monotonic function of the initial mass of the dwarf. The model with the smallest initial mass H1 ends with an apocentric radius of 18 kpc, while the models with larger initial masses end their course closer (H4) as well as further (H8) to the Galactic center.

Fig. 12 shows the evolution of the bound mass as a function of time which is plotted at the apocenters. All models except model H1 have truncated evolutionary curves with the dwarf completely disrupted in a finite computational time.

Figure 13 shows the specific angular momentum as a function of apocentric distance of the sinking dwarf. The evolution of the specific angular momentum of the Hernquist models is not very different from that of the King models.

4 HERNQUIST MODELS VS KING MODELS

We see from our simulations a difference in the behavior of the King and the Hernquist models. The mass loss rate for the King model dwarfs slows down as the bound mass decreases, while for the Hernquist model dwarfs the mass loss rate increase. The Hernquist model dwarfs are more fragile than the King dwarfs regardless of their mass and size because they have shallower central concentration. This, however, only partly explains the fragility of the Hernquist models. We present in this section simple arguments explaining the difference between the King and the Hernquist models.

There are two factors that affect central density distribution of the dwarfs. The gravitational shocks inject energy into the dwarf's central regions. Another factor is an indirect influence of gravitational shocks on the density distribution in the dwarf's central regions. The central density distribution changes as a response to the loss of the outer layers of the dwarf when the dwarf adjusts itself to a new equilibrium. Although these two effects act simultaneously, we estimate them separately in our simple analytical approach.

At the later stages of its evolution, the dwarf orbit has a low inclination toward the disc and the bulge shocking is larger than that from the disc. An approximate expression for the energy injection due to a single bulge shocking (Spitzer 1958) has the form:

$$\Delta E = \frac{M_{\rm dwarf} r_m^2}{3} \left(\frac{2GM_{\rm bulge}}{p^2 V} \right)^2 L(\beta) \qquad (10)$$

Here p, V, r_m, and β are the pericentric distance (~ 1 kpc), the relative velocity (~ 300 km/s), the mean radius of the dwarf and the ratio of the duration of the shock to the stellar orbital period

$$\beta = \frac{p}{V} \frac{v_{\rm rms}(r)}{r}. \qquad (11)$$

The correction factor to the impulsive approximation, $L(\beta)$, is determined by the relative interaction time β such that:

$$L(\beta) = 1, \quad \text{for} \quad \beta \ll 1; \quad L(\beta) \ll 1, \quad \text{for} \quad \beta \gg 1. \qquad (12)$$

Equation (10) can be further approximated by replacing the dependence on $M_{\rm dwarf}$ and r_m^2 in eq. (10) by that of the mass of the dwarf within radius r.

The central density distributions for the King and the Hernquist models can be well approximated by a power-law distribution

$$\rho(r) = \rho_0 \left(\frac{r}{r_0} \right)^n, \quad n = -2 \text{ or } -1, \qquad (13)$$

This profile is a simplification of our King model ($n = -2$)

and the Hernquist model ($n = -1$). Calculating gravitational potential energy for the density distributions (13), we can find a binding energy of the central sphere of radius r for the King and the Hernquist models respectively:

$$E_{\mathrm{bound_K}} = \frac{GM(r)^2}{2r}, \tag{14}$$

and

$$E_{\mathrm{bound_H}} = \frac{GM(r)^2}{3r}, \tag{15}$$

With help of the above expressions, one can write down the fractional energy injection for the King model as:

$$\frac{\Delta E}{E_{\mathrm{bound_K}}} = \frac{16}{3}\frac{M_{\mathrm{bulge}}}{M_{\mathtt{tot}}}\left(\frac{r_{\mathrm{h}}}{r}\right)\frac{r^3}{p^3}\frac{GM_{\mathrm{bulge}}}{pV^2}L(\beta), \tag{16}$$

Here, the mass of the King central sphere of radius r has been expressed using total mass M_{tot}, and the half mass radius r_h: $M(r) = M_{tot}(r/2r_h)$. This gives, for example, for the King model K4:

$$\frac{\Delta E}{E_{\mathrm{bound_K}}} = 3.7\left(\frac{r}{1\mathrm{kpc}}\right)^2 L(\beta) \tag{17}$$

. Similarly, we find for the Hernquist model H4

$$\frac{\Delta E}{E_{\mathrm{bound_H}}} = 5.5\left(\frac{r}{1\mathrm{kpc}}\right) L(\beta) \tag{18}$$

For the accepted parameters, the energy injection is smaller than the binding energy if $r < 0.5$ kpc for the King model, and if $r < 0.2$ kpc for the Hernquist model.

More important effect is a subsequent adjustment of the remnant to a new equilibrium. Let's assume that a Hernquist model is instantaneously stripped to a cutoff radius $r_{cut} < r_0$. In this simplified model we consider mass stripping as the decrease of the cutoff radius r_{cut}. Using the Jeans equation, we can write the expression determining the velocity dispersion of the dwarf at a central region r as a function of cutoff radius r_{cut}:

$$\sigma^2(r,r_{cut}) = \begin{cases} 2\pi G\rho_0 r_0^2\left(1 - r^2/r_{cut}^2\right), & n = -2, \\ 2\pi G\rho_0 r_0 r \ln r_{cut}/r, & n = -1. \end{cases} \tag{19}$$

For the King profile, the central velocity dispersion does not depend much on the cutoff radius r_{cut}, while for the Hernquist profile, the equilibrium velocity dispersion should be lower for smaller r_{cut}. The King model dwarfs keep thus their central density distribution almost intact. The inner regions are close to equilibrium even though the outer layers are removed. On the other hand, the Hernquist model dwarf expands after the shock because it has an excess of internal kinetic energy necessary for equilibrium. This would decrease the density of the dwarf, making it more fragile to future gravitational shocks which leads to a complete disruption of the dwarf in a relatively short time.

5 DISCUSSION

5.1 Living halo

In all of our simulations presented in this paper we assumed that the halo has a fixed potential. This assumption does not allow us to take into account the drag force due to halo dynamical friction that can change the dynamics of the dwarf.

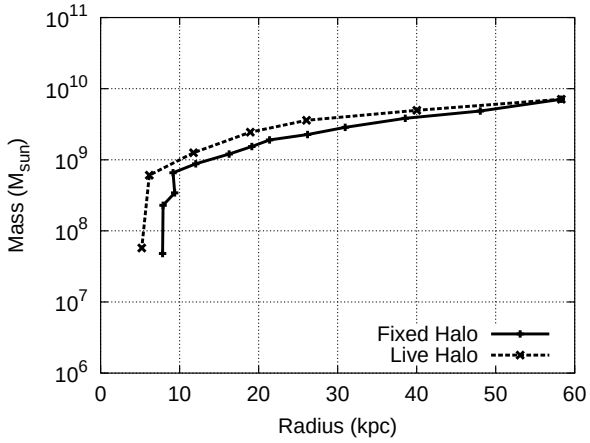

Figure 14. Comparison of the evolutionary histories between models with and without the halo responsiveness. In the apocenter – bound-mass diagram both models take nearly the same track.

For comparison, we ran one simulation with a living halo for dwarf model H4. The halo gravity was calculated with the SCF algorithm (Hernquist and Ostriker 1992). The halo is sampled by 100,000 particles, and the self-consistent dynamics of the whole system is thus treated by a hybrid algorithm, SCF-TREE (Vine and Sigurdsson 1998; Tsuchiya 2002). As expected, we find that the orbit decays faster, and the mass loss rate is higher when compared to that of the models with the fixed halo. For the fixed halo model, the apocenter of the H4-dwarf becomes smaller than 10 kpc after 3 Gyr, while in the living-halo simulation it happens after 1.8 Gyr. However, the evolutionary tracks for the fixed and living halo models are remarkably similar in the bound mass – apocentric distance diagram (Fig. 14). The shock strength depends on the pericentric passage velocity, which in turn determines the apocentric distance of the dwarf orbit. As a result, the bound mass - apocentric distance evolutionary tracks are nearly independent of halo model. Since our basic conclusions are based on the bound mass – apocentric distance diagrams, we correctly predict the final orbit of the remnant.

5.2 ω Centauri

An important application of our simulations is the understanding of the origin of ω Cen. As discussed in Section 4, an ω Cen – like object cannot be created from a dwarf with a highly concentrated King density profile. On the other hand, the dwarfs with Hernquist density profiles exhibit accelerated mass loss and are completely disrupted in a few Gyr. A solution to this dilemma might be the existence of a dense compact nucleus at the center of the Hernquist dwarf. Such a dense compact nucleus can sink together with the disrupting, decaying dwarf and may survive the disruptive encounters with the disc and bulge of the Milky Way. A nucleus with a mass of about $10^7 M_\odot$ does not affect the density distribution of the dwarf, and most of the evolutionary history will be similar to that of a non-nucleated dwarf galaxy. This scenario has been examined in Tsuchiya et al. (2003). We have placed a massive particle of $10^7 M_\odot$ at the center of the Hernquist model H4, and followed its self-consistent

evolution. The nucleus settles into an orbit with apocenter of about 6 kpc, and has a bound mass approaching $10^7 M_\odot$. A nucleus as a single massive particle is obviously a simplification of the model which does not allow us to model realisticallly the dynamics of the stripped nucleus of the dwarf. Although, if the N-body nucleus is compact enough, e.g. can be represented by a King model with a core radius of $\sim$ 10 pc, such a nucleus will survive for a few Gyr on its present orbit. Nucleated dwarf galaxies are common among dwarf galaxies, and such a scenario seems to be a plausible explanation of the origin of ω Cen.

We arbitrarily modeled a compact nucleus by a softened particle with a 35 pc half mass radius, equal to the gravity softening length. Zhao (2003) noticed recently that such a nucleus is more fluffy than the internal central density concentration of the Hernquist model, and might be destroyed by the tidal forces from the surrounding dwarf. A more compact nucleus would obviously remedy the problem. However, with our 35 pc resolution, modeling of a more compact nucleus would not make any difference. Additionally, a compact nucleus will not affect an orbital and mass history of the satellite. We note also that the half-light radius of ω Cen is $4.8'$ (de Marchi, 1999) or about 7 pc.

The subsequent evolution of the proto - Omega Cen object is determined by a number of processes: dynamical friction, evaporation driven by two-body relaxation, gravitational shocks, and mass loss driven by stellar evolution (Fall & Zhang 2001). Our numerical resolution and the assumed model do not allow us to discuss other effects that might affect the future evolution of the remaining object. Gnedin et al. (2002) estimate the mass loss from ω Cen due to the stellar evolution to be $10^{-2} M_{cl}$ Gyr^{-1}. Gravitational shocks which dominate the mass evolution of the massive globular clusters also have a time scale of about a few Gyr (Fall & Zhang 2001). The dynamical friction is negligible for ω Cen. We can speculate therefore that an object which has mass close to that of ω Cen and which has a compact enough density distribution can survive on its orbit during a few Gyr.

Recently, Bekki and Freeman (2003) have discussed a similar model of the origin of ω Cen. They modeled the merger of a nucleated dwarf galaxy with an ancient bulgeless Galaxy whose thin disk has twenty percent of today's thin-disk mass, and included effects of star formation in the dwarf dynamics. They find that the Galactic tidal force induces radial inflow in the center of the dwarf that triggers nuclear starbursts. Bekki and Freeman (2003) conclude therefore that the effecient dwarf nuclear chemical enrichment can be associated with the origin of the observed metal-rich stars in ω Cen.

6 CONCLUSIONS

We have studied the dynamical evolution of a falling dwarf galaxy, which in turn is influenced by the strong gravitational shocks from the bulge and disc of the host galaxy. We focused our study on the mass-loss history, and on the orbital migration of the dwarf. The dwarf galaxy sinks toward the center of the host galaxy due to dynamical friction, which depends on the dwarf's mass. Simultaneously, the dwarf is losing mass due to strong bulge and disc gravitational shocks. As a result, the mass-loss history and orbital decay are closely connected and depend in turn on the internal density distribution of the dwarf. We have examined two different dwarf models, namely a highly-concentrated King model and the Hernquist model. The Hernquist model has a r^{-1} density cusp while the King model has a density profile nearly proportional to r^{-2}. This difference leads to qualitatively different evolutionary courses for the two models. Regardless of the mass and the size, all the King models stop orbital sinking in a few Gyr, once the remnant mass has reached $\sim 10^8\ M_\odot$. The central regions of the King model dwarf remain gravitationally bound, and the remnant continues to orbit for a long time without considerable mass loss. Therefore, if the initial density distribution of the dwarf galaxy is close to isothermal, its remnant can not have a mass much smaller than $10^8\ M_\odot$. On the other hand, the Hernquist model dwarfs keep losing mass even after dynamical friction becomes ineffective. As a consequence, the remnant can be stripped down to a small object. If there is a compact gravitationally bound nucleus in the center of the dwarf with a mass of $\lesssim 10^7\ M_\odot$ and will the size of a globular cluster, it will survive for few Gyr on the present orbit of ω Centauri (e.g., Fall & Zhang 2001). Our results support the capture scenario for the origin of the globular cluster ω Centauri.

ACKNOWLEDGMENTS

The authors thank the referee, M. Wilkinson, for his comments and questions which helped to improve the paper. The authors thank W. van Altena and T. Girard for their comments on the manuscript. TT and VK are grateful for stimulating discussions with Rainer Spurzem, Andreas Just and Michael Fellhauer. TT was supported by Alexander von Humboldt foundation. VK was partly supported by DFG grant 436 RUS 17/112/02.

REFERENCES

Bekki K., Freeman K.C., 2003, MNRAS, 346, L11
Binney J., Tremaine S., 1987, "Galactic dynamics". Princeton University Press, Princeton NJ
Binney J., Merrifield M., 1987, "Galactic astronomy". Princeton University Press, Princeton NJ
Chandrasekhar, S. 1943, ApJ, 97, 255
De Marchi, G., 1999, AJ, 117, 303
Dinescu D. I., Girard T. M., van Altena W. F., 1999, AJ, 117, 1792
Dubinski J., 1996, New Astronomy, 1, 133
Fall, Michael S., Zhang, Quing, 2001, ApJ, 561, 751
Freeman K. C., 2001, In: Deiters S., Fuchs, B., Just, A., Spurzem, R., Wielen, R. (Eds.), "Dynamics of Star Clusters and the Milky Way", p. 43
Freeman, K. 1993, in IAU Symp. 153, Galactic Bulges, ed. H. Dejonghe & H. J. Habing (Dordrecht: Kluwer), 263
Freeman, K., Bland-Hawthorn, J., 2002, ARA, 40, 487
Gnedin, O. Y., Zhao, H. S., Pringle, J. E., Fall, S. M., Livio, M.,& Meylan, G. 2002, ApJ, 568, L23
Hernquist L., 1990, ApJ, 356, 359
Hernquist L., Ostriker J. P., 1992, ApJ, 386, 375

Ibata, R., Irwin, M., Lewis, G.,& Stolte, A. 2001b, ApJ, 547, L133
Kuijken K., Dubinski J., 1995, MNRAS, 277, 1341
Kuijken K., Gilmore G., 1991, ApJL, 367, L9
Searle, L., & Zinn, R. 1978, ApJ, 225, 357
Smith, V. V., Suntzeff, N. B., Cuhna, K., Gallino, R., Busso, M., Lambert, D. L., & Straniero, O. 2000, AJ, 119, 1239
Spitzer, Jr. L., 1958, ApJ, 127, 17
Tsuchiya T., 2002, NewA 7, 293
Tsuchiya T., Dinescu D., Korchagin, V., 2003, ApJL, 589, L29
Vanture, A. D., Wallerstein, G.,& Suntzeff, N. B. 2002, ApJ, 569, 98
Vine S., Sigurdsson S., 1998, MNRAS, 295, 475
Wilkinson M. I., Evans N. W., 1999, MNRAS, 310, 645
Zhao H.S. 2002, in ASP Conf. Ser. 265, Centauri: A Unique Window into Astrophysics, ed. F. van Leeuwen, J. D. Hughes, & G. Piotto (San Francisco: ASP), 391
Zhao H.S. 2003, MNRAS, submitted

This paper has been typeset from a TEX/ LATEX file prepared by the author.